Lanthanides MOFs (Samarium, Europium, and Terbium) Characteristics and Its Possible Potentials

Fahdnul Ashim[1], Agustino Zulys[2] and Jarnuzi Gunlazuardi[3]
{fahdnulashim@gmail.com[1], zulys@sci.ui.ac.id[2], jarnuzi@ui.ac.id[3]}

Department of Chemistry, Faculty of Mathematics and Natural Sciences, University of Indonesia, Depok, 16424, Indonesia

Abstract. The reaction between lanthanide nitrate (Sm, Eu, and Tb) with Na-PTC in DMF and water at 170 ºC solvothermal for 6, 24, and 72 hours resulted in new Ln-MOFs which differed from one another. The new Ln-MOFs were then characterized using FTIR, UV-DRS, TGA, XRD, and SEM-EDX. FTIR and UV-DRS characterization showed that the synthesis time affected the Ln-MOFs structure as seen from the FTIR spectrum shift and changed the band gap value. The three MOFs' XRD patterns showed a polycrystalline structure with about 20 nm with a crystallinity of less than 45% and not found in the X'Pert HighScore 2.1 and Match! 3 software database. This indicates that Ln-MOFs are new compounds. Ln-MOFs are not resistant to high temperatures based on the TGA characterization. The bandgap value for Ln-MOFs is 2.15 - 2.22 eV, so it has the potential as a photocatalyst to degrade dye and produces H_2 gas from the water in the visible area. The use of metal lanthanides allows MOFs to have potential as catalysts in organic reactions. However, this potential must be proven by further experiments.

Keywords: lanthanide nitrate, Ln-MOFs, solvothermal, photocatalyst, lanthanide metal

1 Introduction

Metal-Organic Frameworks (MOFs) was first synthesized in 1995 [1] and are still being developed to this day, both how to synthesize and use them. MOFs are porous materials composed of metal ions or cluster ions linked to organic compounds [2]. MOFs are also known as absorbent coordination polymers (PCPS), a new class of hybrid porous materials with a 3D crystal framework consisting of metal-oxo clusters and organic compounds as a linker [3]. Pores will form when the solvent is removed.

Metals that can make MOFs can be from alkaline earth, transition, and lanthanides [4]. Various organic compounds are used [5] depending on the intended use, physical properties, and desired chemical properties. However, the organic compound must have a functional group with a lone pair of electrons assigned to metal ions and can act as a bridge between metal ions, such as dicarboxylate groups, diamines, diimides, and others.

There are at least 11 methods to synthesize MOFs that have been developed by humans [6], such as solvo/hydrothermal synthesis [7], sonochemistry [8], slow diffusion [9], conventional heating [10], temperature-controlled cooling [11], gel growth crystallization technique [12], microwave synthesis [13], rapid precipitation procedure [14], electrochemical synthesis [6], modulation synthesis [15] and microfluidic synthesis [16]. Among the eleven

AECon 2020, December 19-20, Purwokerto, Indonesia

DOI 10.4108/eai.19-12-2020.2309195

methods, making MOFs more often used is the solvo/hydrothermal method because of its ease in synthesizing MOFs.

Applications from the use of MOFs to date that have been developed by humans are at least 7 [17]. These MOFs include being used as gas storage (9), molecule separation (18), chemical catatalysts [2][15], chemical sensors [19–21], ion exchange (22), drug delivery (23) and photocatalysts (24).

Lanthanide metals is an inner transition metal having 3d-4f orbitals. The presence of an f orbital in the lanthanide metals, which is still empty, can form a coordination number greater than or equal to 9 [25]. The lanthanide metal can be made into MOFs and is known as Ln-MOFs [2]. Ln-MOFs as the catalyst for oxidation and cyanosilylation reactions [2], as a photocatalyst [24], as a chemical sensor [7][21][26–30], and for the degradation of dyes [31].

3,4,9,10-perylene tetracarboxylic acid (PTCA) is an organic compound that has four carboxylic acid groups. PTCA and its derivatives have several uses, such as materials for making organic solar cells [32], electro-oxidation of methanol [33], to detect Pb^{2+} [34], and oxidize water [35].

Based on the many MOFs, metal lanthanides, and PTCA applications, this research aims to synthesize MOFs using metal lanthanides and PTCA with the solvothermal method. The results of the characterization of Ln-MOFs were obtained as a consideration for the application of Ln-MOFs in the next research.

2 Experiment Section

2.1 Chemicals and Characterization Instruments

The chemicals used in this experiment were $Sm(NO_3)_3.6H_2O$, $Eu(NO_3)_3.xH_2O$, $Tb(NO_3)_3.5H_2O$ (Sigma-Aldrich), NaOH (Merck), perylene 3,4,9,10-tetracarboxylic dihydrate (PTCDA) (Sigma-Aldrich), N, N dimethyl-formamide (DMF) (Merck), ethanol (Merck), methanol (Merck), and distilled water.

The synthesized Ln-MOFs were then characterized by Fourier Transform Infra-Red (FTIR) Prestige 21 Shimadzu, Diffuse Reflectance UV-Vis (Shimadzu spectrophotometer 2200A), Thermal Gravimetric Analysis (TGA), X-Ray Powder Diffraction (XRD) Spectrometer Shimadzu 6000 and Scanning Electron Microscope and Energy Dispersive X-ray Spectroscopy (SEM-EDX).

2.2 Synthesis of Na-PTC

The synthesis method of Na-PTC from PTCDA is the modified method from [36]. The ligands to be used for the MOFs synthesis are in the form of salts, not acids. PTCDA (0.5 g, 1.27 mmol) was deposited in 50 ml of distilled water, then NaOH (0.356 g, 8.9 mmol) was added while stirring vigorously, and a solution of sodium perylene tetracarboxylic (Na-PTC) was formed, which was greenish-red. Then filtered and the filtrate obtained is added with excess ethanol to obtain a yellow precipitate. The Na-PTC precipitate was then filtered and washed by ethanol and dried at room temperature for 24 hours. Na-PTC and PTCDA were then compared to their IR spectrum using FTIR.

2.3 Synthesis of Ln-MOFs

The synthesis of Ln-MOFs is the modified method from [36]. $Sm(NO_3)_3.6H_2O$, $Eu(NO_3)_3.xH_2O$ and $Tb(NO_3)_3.6H_2O$ two mmol each (889.0; 676.0 and 870.0 mg) in different containers added with one mmol (516.3 mg) Na-PTC, 4 mL DMF and 11 mL distilled water. Then stirred for 45 minutes, then transferred to Teflon and autoclaved for 6, 24, and 72 hours at 170 ^oC. The crystals formed were filtered and then washed with distilled water and DMF. Then the crystals are dried in an oven at 60 - 80 ^oC for 24 hours.

3 Result and Discussion

3.1 Synthesis results of Na-PTC

The synthesis of Na-PTC ligands from PTCDA was successfully carried out, as evidenced by the ligands color before (red) and after (yellow). NaOH's addition has a different color shown in **Figure 1**. Indicates that chemical bonds are missing or new bonds are formed. The formed or missing chemical bonds are proven by FTIR analysis, which can be seen in **Section 3.3**.

Fig. 1. PTCA (red) and Na-PTC (yellow)

NaOH reacts with an acid anhydride group ($(RCO)_2O$) to form RCOOH and RCOONa. The presence of excess NaOH in the solution makes NaOH react again with the RCOOH group formed in the first reaction. This made the entire $(RCO)_2O$ group turn into RCOONa and was strengthened by the absence of an IR spectrum in the firm and vast area of 2,500 - 3,300 cm^{-1}, indicating the presence of the COOH group.
The purpose of converting PTCDA into Na-PTC (an acid anhydride compound into its salt) is because the solvent medium used to synthesize MOFs uses media containing water. At the same time, PTCDA is insoluble in water, so it needs to be converted into other compounds that are more soluble in water.

3.2 Synthesis results of Ln-MOFs

The synthesis of lanthanide MOFs (Ln-MOFs) was carried out by the solvothermal method at a temperature of 170 ^oC with DMF and water as a solvent. Using more than one type of solvent, the resulting MOFs are expected to be single crystals. The solvent used can

also be replaced according to the form of MOFs want to obtain, such as by using acetone, alcohol, acetonitrile, and others [37]. However, the variation of the solvent was not carried out in this research. The variation used was the length of the MOFs synthesis time with a temperature of 170 ºC.

Before placing it in the ligand mixture oven, the metal salt and the solvent are yellow (**Figure 2**). The yellow color comes from the Na-PTC color, while the metal salts and solvents are colorless. After being put in the oven and drying, the mixture turns red even though the metal is different, as shown in **Figure 3** and **Figure 4**, so it is assumed that Sm-MOFs, Eu-MOFs, and Tb-MOFs have almost the same shape. However, this assumption needs to be proven by further analysis, which can be seen in the section on characterization results with instruments.

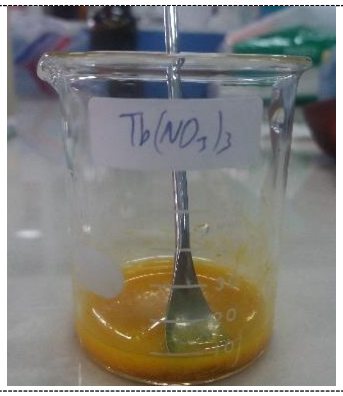

Fig. 2. Ln-MOF before putting it in the oven

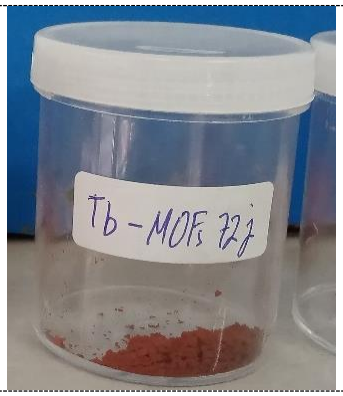

Fig. 3. Ln-MOF after being put in the oven and drying

Fig. 4. Physical form and color of Na-PTC and Ln-MOFs

3.3 FTIR characterization results

Based on the wavenumber value [38], the IR spectrum analysis on the ligands before and after reacting with NaOH (**Figure 5**) shows that new bonds are formed. Some are broken, such as initially there are C - O cyclic anhydride bonds (939 and 1,122 cm^{-1}) and C = O aromatic anhydride in the PTCDA structure (1,757 and 1,774 cm^{-1}) then becomes absent when Na-PTC compounds are formed and changes to C - O carboxylic acids (1,362 cm^{-1}) and C = O carboxylic anions (1,564 cm^{-1}). During the Na-PTC synthesis process, there was no -OH

group, which was proven by the absence of a healthy and board IR spectrum in 2,500 - 3,300 cm^{-1}.

The IR spectrum region is divided into 2, namely the functional group area (3,600 - 1,250 cm^{-1}) and the fingerprint area (1,200 - 600 cm^{-1}) (38). Analysis of the IR spectrum in the functional group region of Ln-MOFs (Ln: Sm, Tb, and Eu) has the same functional group but with slightly different wavenumber values. In the fingerprint area (fingerprint), the IR spectrum has almost the same shape, but the intensity is different. This strengthens the temporary suspicion that the three MOFs have almost the same shape. The comparison of the IR spectrum of the ligands with Ln-MOFs can be seen in **Figure 5**.

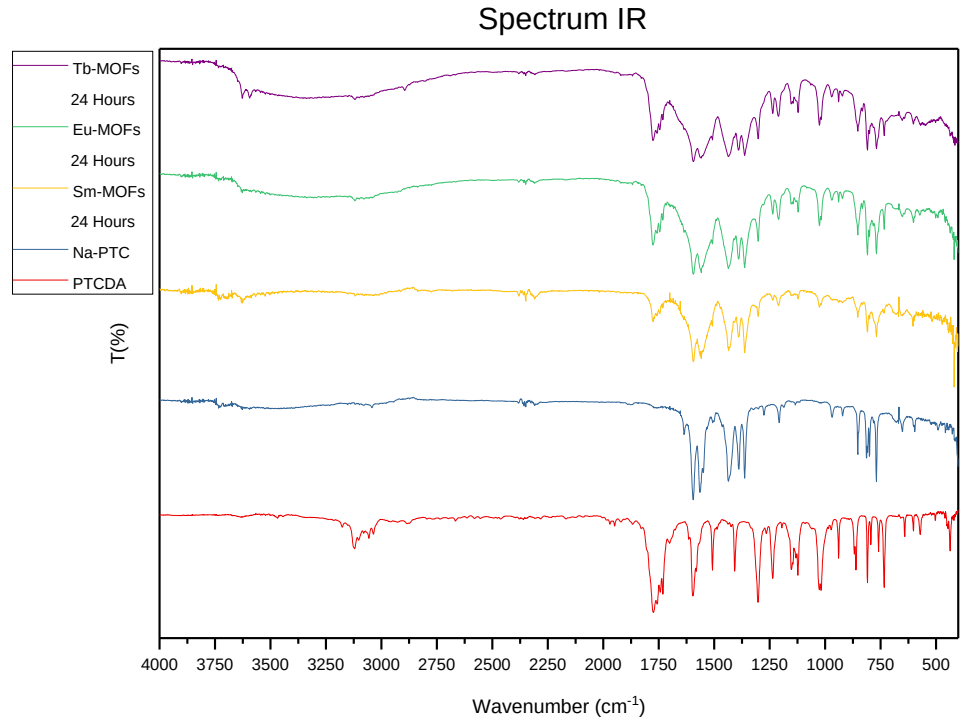

Fig. 5. The comparison of the IR spectrum of the ligands with Ln-MOFs

Comparing the IR Sm-MOFs spectrum with the synthesis time of 6, 24, and 72 hours (**Figure 6**) shows almost the same spectrum shape but with different intensities. The intensity of the C = O bond in the area 1,710 - 1780 cm^{-1} has decreased. This shows that the synthesis time affects the structural shape of the MOFs. This is also experienced by [39] between 10 minutes and 1 hour reaction time at 95 ^{o}C and [40] synthesized MOFs for 24 hours and 48 hours at 150 ^{o}C to produce different forms of MOFs.

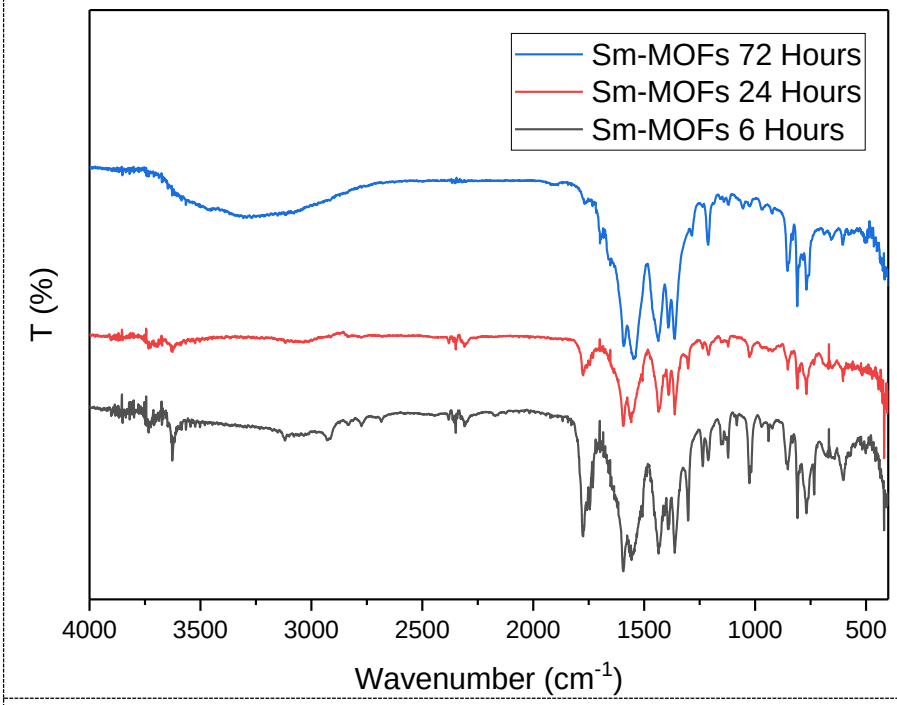

Fig. 6. Comparison of the IR spectrum to the difference in the length of time to synthesize Ln-MOFs

3.4 UV-DRS characterization results

The data obtained from UV-DRS is only in the form of wavelength (λ) and percent reflectance (% R), so it needs to be processed first by using the Kubelka-Munk function (equations 1 - 5) to estimate the band gap value of MOFs. The bandgap value is obtained by plotting the x-axis *h.v* and the y-axis $(F(R).h.v)^2$ with Origin 2017 64-bit software, and the calculation of the Ln-MOFs band gap value can be seen in **Table 1**.

$$h\nu = \frac{1240}{\lambda} \quad (1)$$

$$F(R) = \frac{K}{S} \quad (2)$$

$$K = (1-R)^2 \quad (3)$$

$$S = 2R \quad (4)$$

$$R = \frac{\%R}{100} \quad (5)$$

Information :
h.ν : Energy (eV)
λ : Wavelength (nm)
F (R) : Kubelka-Munk Function
K : Molar absorbance coefficient
S : Scattering factor
R : The reflectance of the material
% R : Percent reflectance of the material

Tabel 1. The result of the Ln-MOFs band gap value

MOFs	Synthesis Time (hours)	Eg_1 (eV)	Eg_2 (eV)
Sm-MOFs	6	2,09	2,02
	24	2,08	2,16
	72	2,00	2,15
Eu- MOFs	24	2,10	2,18
	72	1,93	2,15
Tb- MOFs	24	2,09	2,22
	72	1,97	2,19

Based on the data obtained, Ln-MOFs have 2 Eg (Eg_1 and Eg_2). This is because the UV-DRS spectrum has two peaks that indicate that there is not only one electronic transition. The Eg1 value in Ln-MOFs tends to decrease with increasing synthesis time. The Eg_2 value in Sm-MOFs had increased from 6 hours to 24 hours of synthesis time and then decreased at 72 hours of synthesis time. This reinforces the notion that the length of time for synthesis will affect the structural shape of MOFs.

Ln-MOFs showed a bandgap value greater than 1.23 eV, so that Ln-MOFs has potential as a photocatalyst for water splitting. However, it is necessary to carry out cyclic voltammetry (CV) analysis and the application of photocatalytic water to strengthen the suspicion that the water-splitting reaction can work or not.

Based on the FTIR analysis results and the bandgap values that were not much difference between the synthesis time of 6, 24, and 72 hours, then for further analysis using Ln-MOFs with a synthesis time of 72 hours.

3.5 TGA characterization results

TGA analysis on Sm-MOFs and Tb-MOFs for 72 hours was carried out at a temperature of 25 - 550 ºC. The results obtained are not much different, which can be seen in **Figure 7**. As the TGA analyzer temperature continues to increase, the MOFs' weight continues to decrease from a temperature of 25 ºC to 200 ºC. Sm-MOFs fell by 3.57%, while Tb-MOFs was 4.76%. This shows that MOFs are not resistant to high temperatures.

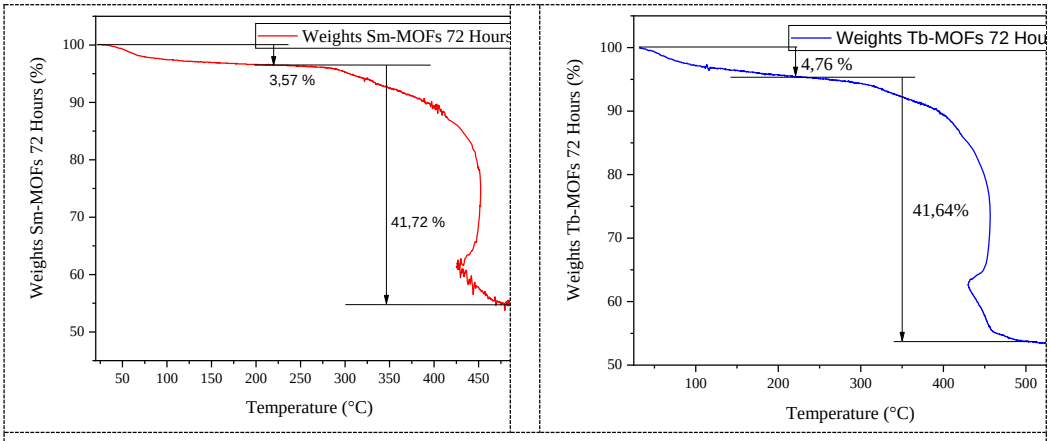

Fig. 7. Results of TGA analysis on Ln-MOFs

When the TGA analyzer temperature was above 225 ºC to 500 ºC, the MOFs' weight was almost half (41.72% and 41.64%). This shows that the organic compounds from MOFs have begun to degrade. After the TGA analysis process is complete, the MOFs' color, which initially was red, turned gray (Sm-MOFs) and brown (Tb-MOFs), as shown in **Figure 8**. Gray and brown colors indicate that metal oxide has formed. Ln-MOFs that have begun to degrade at high temperatures are still suitable if used as photocatalysts to produce H_2 gas from the water with visible light.

Then based on the results of FTIR and UV-DRS analysis, which were not much different between Sm-MOFs, Eu-MOFs, and Tb-MOFs, then the Eu-MOFs were suspected if the TGA analysis was carried out, the results were not much different.

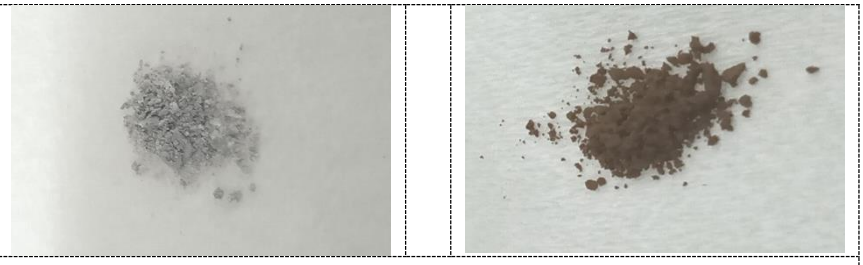

Fig. 8. Color Sm-MOFs (left, gray) and Tb-MOFs (right, brown) after input into the TGA analyzer

3.6 XRD characterization results

Peaks XRD on Sm-MOFs, Eu-MOFs, and Tb-MOFs with a synthesis time of 72 hours can be seen in **Figure 9**. Based on the XRD peaks, the Ln-MOFs synthesized are still polycrystalline. The XRD peaks on Ln-MOFs had the best images of Sm-MOFs 72 hours and had a higher intensity compared to Eu-MOFs and Tb-MOFs with the same synthesis time of 72 hours.

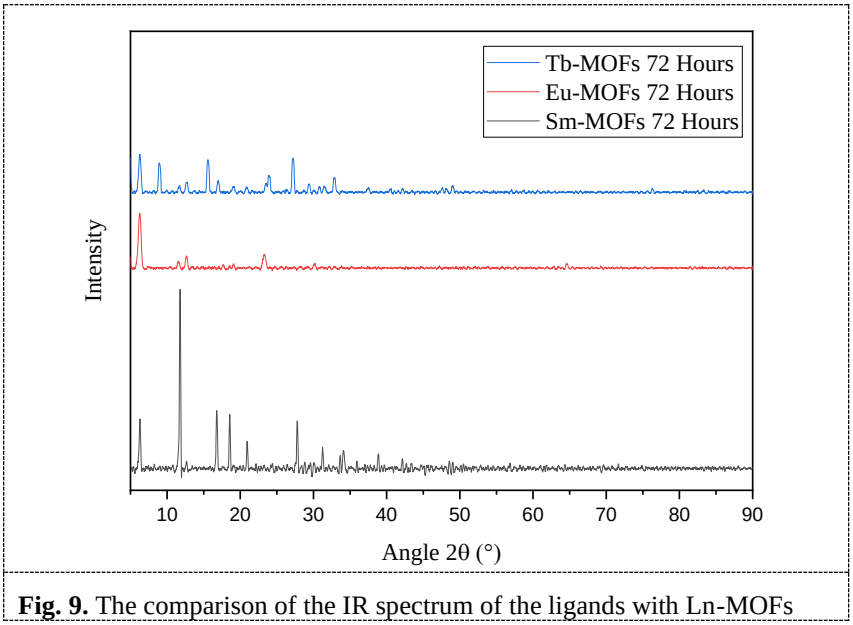

Fig. 9. The comparison of the IR spectrum of the ligands with Ln-MOFs

The XRD peaks pattern from Ln-MOFs was also tried to find using X'Pert HighScore 2.1 and Match! 3 software, but not found in the software database. This shows that Ln-MOFs are new compounds.

Based on the XRD peaks, we can estimate three things: the degree of crystallinity, the crystal size, and the distance between the crystal planes. The peaks are further processed using Origin 2017 64 bit software and Microsoft Excel.

Sm-MOFs 72 hours, Eu-MOFs 72 hours, and Tb-MOFs 72 hours each have a crystallinity of are 23.14%, 30.69%, and 41.07%. The Ln-MOFs crystal size can be estimated using the Scherrer equation, which is equation 6. Mathematically, the mean crystal size was 24.97 nm (Sm-MOFs 72 hours), 18.99 nm (Eu-MOFs 72 hours), and 22.80 nm (Tb-MOFs 72 hours). The complete mathematical crystal size data can be seen in Table 2. Bragg's law estimated the distance between the crystal planes (equation 7) so that the results can be seen in Table 2.

$$D = \frac{K\lambda}{\beta \cos\theta} \tag{6}$$

Information :
D : Crystal size (nm)
K : Scherrer constant (0,9)
λ : Wavelength of X-rays (0.15406 nm)
β : Full Width at Half Maximum (FWHM) (rad)
θ : Peak position (rad)

$$d = \frac{n\lambda}{2 \sin\theta} \tag{7}$$

Information :
λ : Wavelength of X-rays (1,5406 Å)
θ : Peak position (rad)
n : Diffraction order (n = 1)
d : The distance between 2 crystal planes/d-spacing (Å)

Table 2. Crystal Size and d-spacing Ln-MOFs

	Sm-MOFs 72 Hours			Eu-MOFs 72 Hours			Tb-MOFs 72 Hours		
	Peak position 2θ (°)	Crystal size (nm)	d-spacing (Å)	Peak position 2θ (°)	Crystal size (nm)	d-spacing (Å)	Peak position 2θ (°)	Crystal size (nm)	d-spacing (Å)
1	6,27	22,62	14,090	6,25	16,03	14,124	6,30	20,83	14,029
2	11,76	23,70	7,518	11,55	22,73	7,658	8,92	22,24	9,907
3	16,79	24,68	5,277	12,64	21,00	6,996	12,73	20,16	6,949
4	18,56	25,72	4,777	23,29	16,22	3,816	15,57	22,50	5,687
5	20,94	27,56	4,239	-	-	-	16,96	22,95	5,225
6	27,77	25,53	3,210	-	-	-	23,54	26,92	3,776
7	-	-	-	-	-	-	23,86	21,60	3,727
8	-	-	-	-	-	-	27,17	23,11	3,280
9	-	-	-	-	-	-	29,44	24,81	3,032
10	-	-	-	-	-	-	32,88	22,95	2,722

3.7 SEM-EDX characterization results

SEM-EDX analysis on Ln-MOFs shows that the MOFs' shape is still varied, with magnifications of 10,000x, 25,000x, and 50,000x. This is under the results of XRD characterization, which still shows a polycrystalline form. Ln-MOFs at 25,000x magnification have a gravel-like shape, as can be seen in **Figure 10**.

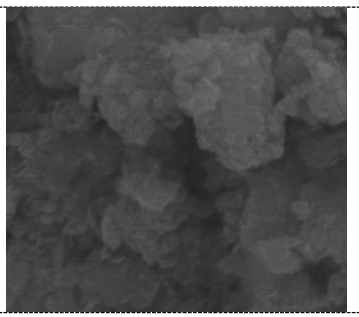
Sm-MOFs 72 Hours

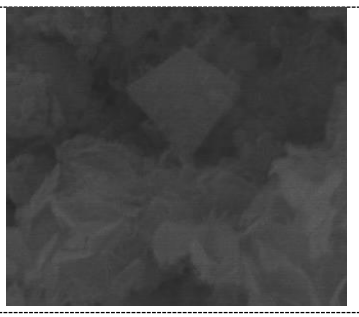
Eu-MOFs 72 Hours

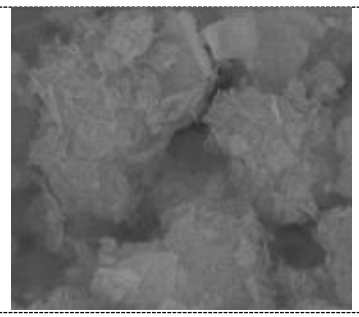
Tb-MOFs 72 Hours

Fig. 10. Morphology of Ln-MOFs at 25,000x magnification

The lanthanide group elements are already present in Ln-MOFs. The elements of carbon and oxygen were also detected. This element comes from the ligands used. Other elements detected with small intensity come from impurities in the SEM-EDX instrument. The element intensity detected in Ln-MOFs can be seen in **Figure 11**.

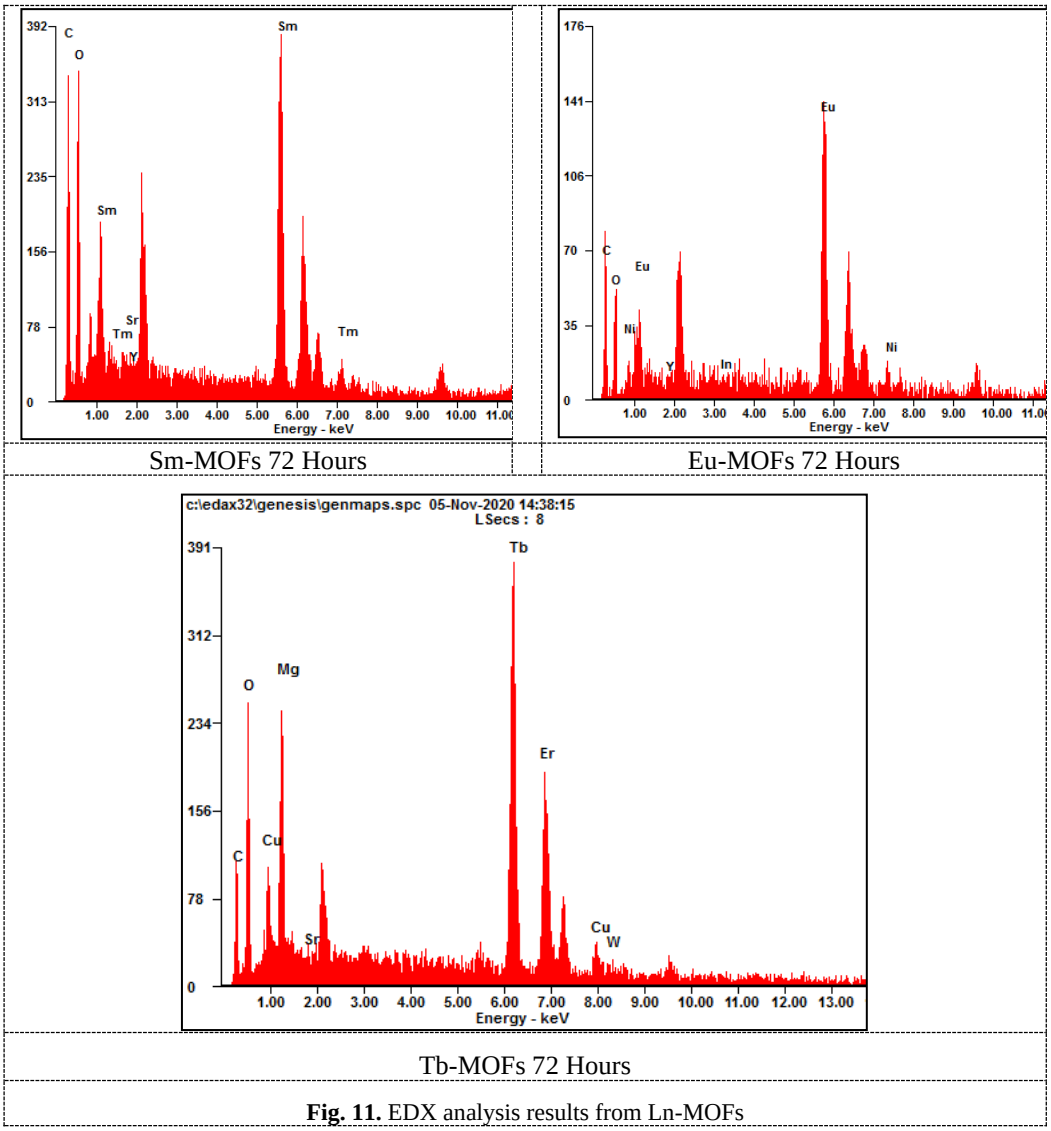

Sm-MOFs 72 Hours | Eu-MOFs 72 Hours

Tb-MOFs 72 Hours

Fig. 11. EDX analysis results from Ln-MOFs

3.8 Potential applications of Ln-MOFs

Based on the three Ln-MOFs characterization results, Ln-MOFs have the potential as a photocatalyst to produce H_2 gas from water and degrade dye. MOFs can act as photocatalysts,

and it can be seen from the band gap value. If the bandgap value is more significant than 3.1 eV, it is irradiated with UV light, and if it is less than 3.1 eV, visible light can be used [41]. The potential of Ln-MOFs in this research as a photocatalyst to produce H_2 gas from water and degrade dye can be seen in Table 3 and Table 4.

The presence of d and f orbitals causes complex compounds of lanthanides to function as Lewis acids to be used as catalysts in the Fridel − Crafts, Diels − Alder, aldol, allylation, and Michael addition reactions [2]. The synthesis reaction of organic compounds with the help of Ln-MOFs can be carried out at room temperature up to 80 ºC [42]. Based on these, the three new Ln-MOFs that were successfully synthesized have potential as catalysts in organic compounds. However, this potential must be tried experimentally first.

Table 3. MOFs research as a photocatalyst to produce H_2 gas from water

MOFs	Band Gap (eV)	Photosensitizers	Sacrificial agents	Cocatalysts	Irradiation	H_2 Production rate ($\mu mol\ g^{-1}h^{-1}$)	Ref.
PCN-415-NH_2	1.99	-	TEOA	Pt	Visible	594	[43]
Cu-I-bpy	2.05	-	TEA	-	UV	7,09	[44]
MOF-199/Ni	2.48	Eosin Y	TEOA	-	Visible	8000	[45]
{[$Tb_2Cu_5(OH)_2$(pydc)$_6(H_2O)_8$]·I_8}	2.82	-	MeOH	-	UV	2105.0	[24]
Ln-MOFs (Ln : Sm, Eu and Tb)	1.93 – 2.22	Na-PTC	-	-	-	-	This Research

Table 4. MOFs research as a photocatalyst degradation of dyes

MOFs	Band Gap (eV)	Dye	Irradiation	Ref.
BR14@HKUST-1	-	RB13	Visible	[46]
MIL-53(Fe)	-	RhB	Visible	[47]
MIL-53(Al)	3.87	MB	Visible	[48]
MIL-53(Cr)	3.20	MB	Visible	[48]
MIL-53(Cr)	2.72	MB	Visible	[48]
Ln-MOFs (Ln: Sm, Eu, and Tb)	1.93 – 2.22	-	-	This Research

4 Conclusions

A total of 3 new Ln-MOFs were successfully synthesized. The Ln-MOFs have almost the same functional groups and band gap values but are still polycrystals with the largest crystal size owned by Sm-MOFs, then Tb-MOFs, and Eu-MOFs. The newly synthesized Ln-MOFs have the potential as photocatalysts to produce H_2 gas from water; photocatalysts degrade dyes and catalysts in the synthesis of organic compounds.

Acknowledgments

The author is grateful for the funding support for this research from the Directorate of Research and Development (Risbang), the University of Indonesia, from the UI Research Grant (*Hibah Riset* UI) 2020 and confirms that there is no conflict of interest were declared regarding this research.

References

[1] Yaghi OM, Li H. Hydrothermal Synthesis of a Metal-Organic Framework Containing Large Rectangular. J Am Chem Soc. 1995;117:10401–2.

[2] Pagis C, Ferbinteanu M, Rothenberg G, Tanase S. Lanthanide-Based Metal Organic Frameworks: Synthetic Strategies and Catalytic Applications. ACS Catal. 2016;6:6063−6072.

[3] Horiuchi Y, Toyao T, Saito M, Mochizuki K, Iwata M, Higashimura H, et al. Visible-Light-Promoted Photocatalytic Hydrogen Production by Using an Amino-Functionalized Ti (IV) Metal − Organic Framework. J Phys Chem C. 2012;116:20848−20853.

[4] Corkery RW. Metal organic framework (MOF) liquid crystals . 1D , 2D and 3D ionic coordination polymer structures in the thermotropic mesophases of metal soaps , including alkaline earth , transition metal and lanthanide soaps. Curr Opin Colloid Interface Sci. 2008;13(2008):288–302.

[5] Stock N, Biswas S. Synthesis of Metal-Organic Frameworks (MOFs): Routes to Various. Chem Rev. 2012;112:933–69.

[6] Hu M-L, Masoomi MY, Morsali A. Template strategies with MOFs. Coord Chem Rev [Internet]. 2019;387(2019):415–35. Available from: https://doi.org/10.1016/j.ccr.2019.02.021

[7] Qu S, Song N, Xu G, Jia Q. A ratiometric fluorescent probe for sensitive detection of anthrax biomarker based on terbium-covalent organic polymer systems. Sensors Actuators B Chem [Internet]. 2019;290(2019):9–14. Available from: https://doi.org/10.1016/j.snb.2019.03.110

[8] Safarifard V, Morsali A. Applications of ultrasound to the synthesis of nanoscale metal – organic coordination polymers. Coord Chem Rev [Internet]. 2015;292(2015):1–14. Available from: http://dx.doi.org/10.1016/j.ccr.2015.02.014

[9] Xin Z, Bai J, Shen Y, Pan Y. Hierarchically Micro- and Mesoporous Coordination Polymer Nanostructures with High Adsorption Performance. Cryst Growth Des. 2010;10(6):2451–2454.

[10] Bagheri M, Masoomi MY, Morsali A, Schoedel A. Two Dimensional Host − Guest Metal − Organic Framework Sensor with High Selectivity and Sensitivity to Picric Acid. ACS Appl Mater Interfaces. 2016;8:21472−21479.

[11] Chen W, Wang M, Liu X, Guo G, Huang J. Investigations of Group 12 (IIB) Metal Halide/Pseudohalide-Bipy Systems: Syntheses, Structures, Properties, and TDDFT Calculations (Bipy=2,2′-bipyridine or 4,4′-bipyridine). Cryst Growth Des. 2006;6(10):2289–300.

[12] Khanjani S, Morsali A. A new nano-particles La III compound as a precursor for preparation of La2O2(SO4) nano-particles. J Mol Struct [Internet]. 2009;935(2009):27–31. Available from: http://dx.doi.org/10.1016/j.molstruc.2009.06.035

[13] Taylor-pashow KML, Rocca J Della, Xie Z, Tran S, Lin W. Postsynthetic

Modifications of Iron-Carboxylate Nanoscale Metal - Organic Frameworks for Imaging and Drug Delivery. J AM CHEM SOC. 2009;131:14261–3.
[14] Shi N, Xie L, Sun H, Duan J, Yin G, Xu Z, et al. Facile synthesis of shape and size tunable porphyrinoid coordination polymers : from copper porphyrin nanoplates to microspindles. Chem Commun. 2011;47:5055–7.
[15] Masoomi MY, Beheshti S, Morsali A. Shape Control of Zn(II) Metal − Organic Frameworks by Modulation Synthesis and Their Morphology-Dependent Catalytic Performance. Cryst Growth Des. 2015;15:2533−2538.
[16] Puigmartí-luis J, Rubio-martínez M, Hartfelder U, Imaz I, Maspoch D, Dittrich PS. Coordination Polymer Nanofibers Generated by Microfluidic. J Am Chem Soc. 2011;133:4216–9.
[17] Farha OK, Hupp JT. Rational Design, Synthesis, Purification, and Activation of Metal-Organic Framework Materials. Acc Chem Res [Internet]. 2010;43(8):1166–75. Available from: https://pubs.acs.org/doi/10.1021/ar1000617
[18] Li J-R, Kuppler RJ, Zhou H-C. Selective gas adsorption and separation in metal – organic frameworks. Chem Soc Rev. 2009;38:1477–1504.
[19] Zhang Y, Yan B. A ratiometric fluorescent sensor with dual response of Fe3+ / Cu2+ based on europium post-modified sulfone-metal-organic frameworks and its logical application. Talanta [Internet]. 2019;197(2019):291–8. Available from: https://doi.org/10.1016/j.talanta.2019.01.037
[20] Liu W, Wang Y, Song L, Silver MA, Xie J, Zhang L, et al. Efficient and selective sensing of Cu^{2+} and UO_2^{2+} by a europium metal-organic framework. Talanta [Internet]. 2019;196(2019):515–22. Available from: https://doi.org/10.1016/j.talanta.2018.12.088
[21] Cui Y, Chen F, Yin X-B. A ratiometric fluorescence platform based on boric-acid-functional Eu-MOF for sensitive detection of H_2O_2 and glucose ☆. Biosens Bioelectron [Internet]. 2019;135(2019):208–15. Available from: https://doi.org/10.1016/j.bios.2019.04.008
[22] Min KS, Suh MP. Silver (I) - Polynitrile Network Solids for Anion Exchange : Anion-Induced Transformation of Supramolecular Structure in the Crystalline State. J Am Chem Soc. 2000;122:6834–40.
[23] Hanif QA, Nugraha RE, Lestari WW. Kajian Metal – Organic Frameworks (MOFs) sebagai Material Baru Pengantar Obat. ALCHEMY J Penelit Kim. 2018;14(1):16–36.
[24] Hu X-L, Sun C-Y, Qin C, Wang X-L, Wang H-N, Zhou E-L, et al. Iodine-templated assembly of unprecedented 3d–4f metal–organic frameworks as photocatalysts for hydrogen generation. Chem Commun. 2013;49:3564–6.
[25] Atkins P, Overton T, Rourke J, Weller M, Armstrong F, Hagerman M. Inorganic Chemistry. 5th ed. New York: W. H. Freeman and Company; 2009. 206–208 p.
[26] Liu Y, Wygant BR, Mabayoje O, Lin J, Kawashima K, Kim J, et al. Interface Engineering and its Effect on WO3 - Based Photoanode and Tandem Cell. ACS Appl Mater Interfaces. 2018;10:12639−12650.
[27] Qi Z, Wang L, You Q, Chen Y. PA-Tb-Cu MOF as luminescent nanoenzyme for catalytic assay of hydrogen peroxide. Biosens Bioelectron [Internet]. 2017;96(2017):227–32. Available from: http://dx.doi.org/10.1016/j.bios.2017.05.013
[28] Eskandari H, Amirzehni M, Asadollahzadeh H, Hassanzadeh J, Eslami PA. MIP-capped terbium MOF-76 for the selective fluorometric detection of cefixime after its preconcentration with magnetic graphene oxide. Sensors Actuators B Chem [Internet]. 2018;275(2018):145–54. Available from: https://doi.org/10.1016/j.snb.2018.08.050

[29] Guo H, Zhu S, Cai D, Liu C. Fabrication of ITO glass supported Tb-MOF film for sensing organic solvent. Inorg Chem Commun [Internet]. 2014;41(2014):29–32. Available from: http://dx.doi.org/10.1016/j.inoche.2013.12.028

[30] Chai H, Ren Y, He H, Wang Z, Zhang Y, Gao L. A microporous Tb-MOF luminescent sensor based on a flexible tricarboxylate for highly sensitive detection of acetone and Fe^{3+} ions in aqueous and isopropanol. J Solid State Chem [Internet]. 2019;271(2019):162–7. Available from: https://doi.org/10.1016/j.jssc.2018.12.048

[31] Wang J, Si P, Liu M, Chen Y, Yu S, Lu M, et al. Selective fluorescent sensing and photodegradation properties of Tb (III) -based MOFs with different bulky backbone ligands. Polyhedron. 2019;157(2019):63–70.

[32] Shibano Y, Imahori H, Adachi C. Organic Thin-Film Solar Cells Using Electron-Donating Perylene Tetracarboxylic Acid Derivatives. J Phys Chem C [Internet]. 2009;113(34):15454–66. Available from: https://pubs.acs.org/doi/10.1021/jp9045726

[33] Wu B, Hu D, Kuang Y, Yu Y, Zhang X, Chen J. High dispersion of platinum–ruthenium nanoparticles on the 3,4,9,10-perylene tetracarboxylic acid-functionalized carbon nanotubes for methanol electro-oxidation. Chem Commun. 2011;47:5253–5.

[34] Huang L, Yang L, Zhu C, Deng H, Liu G, Yuan Y. Methylene blue sensitized photoelectrochemical biosensor with 3,4,9,10-Perylene tetracarboxylic acid film as photoelectric material for highly sensitive Pb^{2+} detection. Sensors Actuators B Chem [Internet]. 2018;274(2018):458–63. Available from: https://doi.org/10.1016/j.snb.2018.07.135

[35] Zheng R, Zhang M, Sun X, Chen R, Sun X. Perylene-3,4,9,10-tetracarboxylic acid accelerated light-driven water oxidation on ultrathin indium oxide porous sheets. Appl Catal B Environ [Internet]. 2019;254(2019):667–76. Available from: https://doi.org/10.1016/j.apcatb.2019.05.003

[36] Sun X, Yu Q, Zhang F, Wei J, Yang P. A dye-like ligand-based metal-organic framework for efficient photocatalytic hydrogen production from aqueous solution. Catal Sci Technol. 2016;6:3840–4.

[37] Seetharaj R, Vandana P V., Arya P, Mathew S. Dependence of solvents , pH , molar ratio and temperature in tuning metal organic framework architecture. Arab J Chem [Internet]. 2019;12(2019):295–315. Available from: https://doi.org/10.1016/j.arabjc.2016.01.003

[38] Shriner RL, Hermann CKF, Morrill TC, Curtin DY, Fuson RC. The Systematic Identification of Organic Compounds. 8th ed. New Jersey: John Wiley & Sons, Inc; 2004. 200–227 p.

[39] Burrows AD, Frost CG, Kandiah M, Keenan LL, Mahon MF, Savarese TL, et al. The effect of reaction conditions on the nature of cadmium 1 , 3 , 5-benzenetricarboxylate metal – organic frameworks. Inorganica Chim Acta [Internet]. 2011;366(2011):303–9. Available from: http://dx.doi.org/10.1016/j.ica.2010.11.025

[40] Mahata P, Prabu M, Natarajan S. Role of Temperature and Time in the Formation of Infinite - M - O - M - Linkages and Isolated Clusters in MOFs : A Few Illustrative Examples. Inorg Chem. 2008;47(19):8451–63.

[41] Gautam S, Agrawal H, Thakur M, Akbari A, Sharda H, Kaur R, et al. Metal oxides and metal organic frameworks for the photocatalytic degradation: A review. J Environ Chem Eng [Internet]. 2020;8(2020):103726. Available from: https://doi.org/10.1016/j.jece.2020.103726

[42] Alzamly A, Bakiro M, Hussein Ahmed S, Alnaqbi MA, Nguyen HL. Rare-earth metal–organic frameworks as advanced catalytic platforms for organic synthesis.

Coord Chem Rev [Internet]. 2020;425(2020):213543. Available from: https://doi.org/10.1016/j.ccr.2020.213543

[43] Yuan S, Qin J, Xu H, Su J, Rossi D, Chen Y, et al. [Ti8Zr2O12(COO)16] Cluster: An Ideal Inorganic Building Unit for Photoactive Metal−Organic Frameworks. ACS Cent Sci. 2018;4:105−111.

[44] Shi D, Zheng R, Sun M-J, Cao X, Sun C-X, Cui C-J, et al. Two-in-One: Semi-Conductive Copper(I)–Organic Frameworks for Efficient Light-Driven Hydrogen Generation Without Additional Photosensitizers and Cocatalysts. Angew Chem Int Ed. 2017;56(46):14637–41.

[45] Zhao J, Wang Y, Zhou J, Qi P, Li S, Zhang K, et al. A copper(II)-based MOF film for highly efficient visible-light-driven hydrogen production†. J Mater Chem A. 2016;4:7174–7.

[46] Zhang LH, Zhu Y, Lei BR, Li Y, Zhu W, Li Q. Trichromatic dyes sensitized HKUST-1 (MOF-199) as scavenger towards reactive blue 13 via visible-light photodegradation. Inorg Chem Commun [Internet]. 2018;94(2018):27–33. Available from: https://doi.org/10.1016/j.inoche.2018.05.027

[47] Nguyen VH, Bach LG, Bui QTP, Nguyen TD, Vo DVN, Vu HT, et al. Composite photocatalysts containing MIL-53(Fe) as a heterogeneous photo-Fenton catalyst for the decolorization of rhodamine B under visible light irradiation. J Environ Chem Eng [Internet]. 2018;6(2018):7434–41. Available from: https://doi.org/10.1016/j.jece.2018.10.020

[48] Du JJ, Yuan YP, Sun JX, Peng FM, Jiang X, Qiu LG, et al. New photocatalysts based on MIL-53 metal-organic frameworks for the decolorization of methylene blue dye. J Hazard Mater [Internet]. 2011;190(2011):945–51. Available from: http://dx.doi.org/10.1016/j.jhazmat.2011.04.029